Adsorption and reaction of sulfachloropyridazine sulfonamide antibiotic on a high silica mordenite: A structural and spectroscopic combined study

Annalisa Martucci [a], Mauro Andrea Cremonini [b], Sonia Blasioli [c], Lara Gigli [d], Giorgio Gatti [e], Leonardo Marchese [e], Ilaria Braschi [c,e,*]

[a] Dipartimento di Fisica e Scienze della Terra, Università di Ferrara, Via Saragat, 1, 44100 Ferrara, Italy
[b] Agilent Technologies Italy, Via Gobetti 2/C, Cernusco S/N, Milano, Italy
[c] Dipartimento di Scienze Agrarie, Università di Bologna, Viale Fanin, 44, 40127 Bologna, Italy
[d] Dipartimento di Scienze Chimiche e Geologiche, Università di Modena e Reggio Emilia, Largo Santa Eufemia, 19, 41100 Modena, Italy
[e] Dipartimento di Scienze e Innovazione Tecnologica and Centro Interdisciplinare Nano-SiSTeMI, Università del Piemonte Orientale "Amedeo Avogadro", Viale Michel 11, 15121 Alessandria, Italy

ARTICLE INFO

ABSTRACT

Owing to their acidic nature, sulfonamide antibiotics concentrate in anionic form in water bodies where they can remain unchanged for long periods of time, accounting for great concern for antibiotic-resistance issues. In this study the removal of sulfachloropyridazine (4-amino-N-(6-Cl-3-pyridazinyl)benzene sulfonamide) antibiotic from water by adsorption on a high silica mordenite with channel window dimension comparable to that of the antibiotic, and with a significant concentration of internal silanol groups due to the dealumination process, was investigated. The adsorption of sulfachloropyridazine by mordenite at room temperature was completed within 4 h with the maximal amount of adsorbed antibiotic of 15.1% zeolite dry weight. The desorption trials elucidated the irreversibility of the adsorption process. The embedding of sulfachloropyridazine into mordenite channels was confirmed by a combined XRPD and FTIR study. Rietveld structure refinement revealed that the incorporation of sulfachloropyridazine molecules caused changes in the dimension of the zeolite channel systems, when compared to the parent zeolite, and a close vicinity of the heterocycle ring nitrogen to the oxygens of mordenite side pocket. FTIR revealed a strong perturbation of the vibrational modes of both the pyridazinyl ring and mordenite silanol groups upon antibiotic adsorption. When the adsorption was conducted at 65 °C, an unfavourable temperature effect was highlighted and, interestingly, sulfachloropyridazine transformed with 100% selectivity to 4-amino-N-(6-hydroxyl-3-pyridazinyl)benzene sulfonamide. A nucleophilic aromatic substitution (S_NAr) mechanism was suggested for the formation of the reaction product. It is proposed that the H-bond between mordenite silanol groups and pyridazine nitrogen atom, clearly detected by FTIR, stabilize in the ring partial positive charges favouring the displacement of the chloride leaving group.

© 2012 Elsevier Inc. All rights reserved.

1. Introduction

Mordenite is a natural or synthetic zeolite (idealised chemical composition $Na_8Al_8Si_{40}O_{96}\cdot24H_2O$) widely used catalyst for cracking, (hydro)isomerisation, and alkylation reactions in the petrochemical industry [1]. Its framework can be built up by the assembly of single 6 membered ring (MR) sheets linked by single 4MR, or else by a combination of 5-1 secondary building units. Mordenite contains sinusoidal channels with limiting 8MR windows parallel to **b** axis that intersect with one-dimensional 8MR and 12MR channels parallel to **c** axis. The 12MR channels (aperture 7 Å × 6.5 Å) wall has side pockets in the [0 1 0] direction. Each side pocket connects through 8MR rings (aperture 3.4 Å × 4.8 Å) the 12MR channel to a distorted 8MR channel running parallel to [0 0 1] (aperture 5.7 Å × 2.6 Å).

In general, mordenite shows limited diffusion and undergoes rapid deactivation due to its monodimensional pore system. In the absence of structural defects, side pockets are inaccessible to molecules larger than methane [2]. To overcome the diffusion problem, additional meso and microporosity is created by dealumination and/or steaming processes. Dealumination of mordenite leads to an enlargement of the main channels and, even more pronounced, the side pockets [3]. Only a few studies on structural properties of partially dealuminated mordenite up to Si/Al = 50 have been done [1,4–5] and even less on highly dealuminated samples [6].

To date, studies and applications dealing with adsorption of pollutants in high silica zeolites from aqueous media are limited [6–13]. As the research in this field is at the beginning, more efforts must be done in order to improve general knowledge on sorbents available for water bodies depollution.

Since their discovery in 30s, sulfonamide antibiotics (sulfa drugs) have been widely used for treatment and prophylaxis against bacterial infections, as well as health promoters, with limited or null regard of their diffusion in unconfined environments. The environmental behaviour of sulfa drugs is mainly characterised by the acidic nature of their sulfonamide group that may occur as anionic form under neutral/slightly basic pH conditions in soil–water system [14]. Some studies on the mobility of sulfonamides in soils demonstrated their attitude to be leached along the soil profile [15] because of the net negative charge always present on the surface of soil particles [16,17]. When the antibiotic administration takes place directly in water, for instance in the case of aquaculture treatment, soil depurative and filtering activity is by-passed and the sulfonamide effect on the environment is even worse [18]. Sulfonamides are among the antibiotics with the highest capability to induce high level of resistance in bacteria through a by-pass mechanism [19].

The delay in the development of new antibiotic compounds, their massive (very often unneeded) use especially as growth promoters, the lack of cleaning-up procedures of sewage and manure disposals where antibiotics usually concentrate once released by treated organisms, result in the diffusion of bacteria resistant to antibiotics all over the world. A cheap and environmentally friendly material with good sorbent properties for sulfonamides has been recently proposed [7,8] aiming to find out cleaning-up procedure to reduce the level of antibiotics into water bodies. A zeolite Y with 200 silica/alumina ratio adsorbs from water sulfonamide antibiotics up to 25% zeolite dry weight with a favourable kinetics (90% in less than 1 min). The embedding of sulfonamides into zeolite cages was revealed by unit cell parameter variation and structural deformation of zeolite Y [7]. Multiple weak H-bonds and van der Waals type interactions between sulfonamides and zeolite Y wall are responsible for the complete extraction from water of sulfa drugs [8].

In the present study, a commercial high silica zeolite mordenite is presented for its favourable adsorption properties towards sulfachloropyridazine sulfonamide antibiotic. The type of interactions involved during the adsorption of sulfachloropyridazine into mordenite has been enlightened respectively by XRPD analysis and FTIR spectroscopy. Moreover, we report on unprecedented NMR evidences that this mordenite transforms with 100% selectivity sulfachloropyridazine into a different sulfonamide structure.

2. Experimental

2.1. Materials

Sulfachloropyridazine (4-amino-N-(6-Cl-3-pyridazinyl)benzene sulfonamide, SC) was purchased as analytical standards by Dr. Ehrenstorfer GmbH (Germany) with a purity of 98.0%. This antimicrobial agent has been chosen because of its widespread consumption and predominant occurrence in water bodies and soils [20–22]. The chemical structure of sulfachloropyridazine along with some chemical and physical properties are shown in Table 1.

A solution of antibiotic at maximal solubility was prepared by adding sulfachloropyridazine to distilled water in amounts exceeding that required to saturate the solution. The suspension was sonicated for 15 min, shaken at 50 °C for 30 min and, after cooling at room temperature (RT), filtered through 0.45 µm

Durapore® membrane filters to eliminate the undissolved solute from the solution. The solubility of the antibiotic, measured by means of high performance liquid chromatography (HPLC), was 173.6 ± 7.7 µM.

Mordenite zeolite powder with 200 SiO_2/Al_2O_3 ratio, was purchased (code HSZ-690HOA) in its protonated form from Tosoh Corporation (Japan): this sample is hereafter named HS-MOR. Mordenite powder with 20 SiO_2/Al_2O_3 ratio was purchased in ammonium form (code CBV21A) from Zeolyst International as a reference material. This mordenite was transformed into the protonic form by calcination at 600 °C for 4 h in a static oven: this reference sample is hereafter named R-MOR.

2.2. Surface area and porosimetric analysis

Specific surface area and pore volume of both mordenite samples were determined by nitrogen adsorption at liquid nitrogen temperature (−196 °C) in the pressure range 1×10^{-6}–760 Torr (1 Torr = 133.33 Pa) using an Autosorb-1-MP (Quantachrome Instruments, Boynton Beach, USA). Before adsorption, the samples were outgassed for 1 h at 90 °C, 1 h at 130 °C, and finally 16 h at 300 °C under high vacuum conditions (final pressure 1×10^{-8} Torr). External surface areas were obtained applying the Brunauer–Emmett–Teller (BET) method. An analysis of the pore distribution was not attempted for N_2 physisorption does not allow obtaining detailed information on the microporosity. However, the cumulative pore volume as a function of the pore size diameter was obtained analysing the desorption branch of the N_2 physisorption with a non-local density functional theory (NLDFT) and using a cylindrical pore model that allows a quantification of both micro- and mesoporosity [23]. Although the micropore volumes are not accurate enough for the use of N_2 instead of Ar probe, the comparison between the two mordenite samples provides precious information.
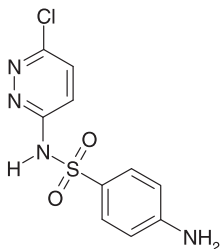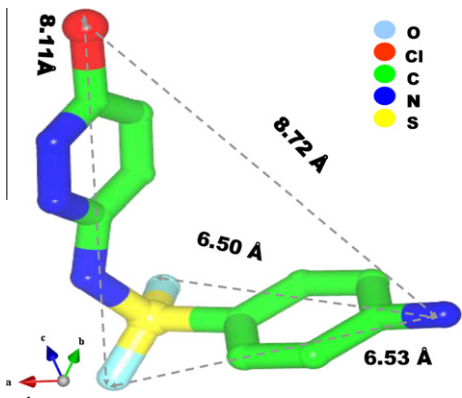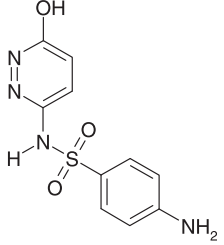
2.3. Thermogravimetric analysis

Thermogravimetric analyses (TGA) were carried out using a TGDTA92 instrument (SETARAM, France). About 20 mg of samples were weighed into an aluminium crucible and heated continuously from 30 °C to 800 °C at a heating rate of 10 °C min^{-1} under air flow of 8 L h^{-1}. Calcined kaolinite was used as a reference material. The furnace was calibrated using an indium transition temperature. The weight losses were referred to the weight of the air-dried sample.

2.4. X-ray diffraction

Powder diffraction data of mordenite before (HS-MOR) and after sulfachloropyridazine adsorption (HS-MOR/SC) were collected using a Bruker D8 Advance Diffractometer equipped with Sol-X detector, (CuK$_{\alpha1,\alpha2}$ radiation) using Cu K$_{\alpha1,\alpha2}$ radiation in the 3–110° 2θ range and a counting time of 12 s step^{-1}. The HS-MOR/SC diffraction pattern was firstly indexed using the DICVOL program [24] an orthorhombic cell [$a = 18.067$ Å, $b = 20.234$ Å, $c = 7.454$ Å, $V = 2724.8$ Å^3]. No violation of the C-centring systematic absences was observed. Both Rietveld structure refinements were performed in the $Cmc2_1$ space group, using the GSAS package [25] with the EXPGUI interface [26] starting from the framework atoms reported by Alberti et al. (1986) [27]. All tetrahedral sites were modelled with Si atoms, neglecting the amount of Al atoms. The Bragg peak profile was modelled using a pseudo-Voigt function [28] with 0.01% cut-off peak intensity. The background curve was fitted using a Chebyschev polynomial with 20 variable coefficients. The scale factor, the 2θ-zero shift and unit-cell parameters were accurately refined into the data set pattern. Occupancy

Table 1
Structure and selected physical and chemical characteristics of sulfachloropyridazine and its reaction product.

Structure	IUPAC name (commercial name)	Molecular weight (g mol^{-1})	pK$_a$	3D structure[a]
Cl ... NH$_2$ (sulfachloropyridazine structure)	4-amino-*N*-(6-*Cl*-3-pyridazinyl)benzene sulfonamide (sulfachloropyridazine)	284.7	5.5[b]	8.11Å, 8.72 Å, 6.50 Å, 6.53 Å; O, Cl, C, N, S
OH ... NH$_2$ (reaction product structure)	4-amino-*N*-(6-hydroxyl-3-pyridazinyl)benzene sulfonamide	266.3	n.d.	n.d.

n.d. not determined.
[a] Reference for 3D structure is Tan et al., 2005.
[b] Reference for pKa of sulfachloropyridazine amide group is Ishihama et al., 2002.

factors and isotropic displacement factors (one for each tetrahedral site and framework oxygen atom), were varied in alternate cycles. The SC molecule sites were determined analysing the Fourier and the difference Fourier maps focusing on the large 12MR channel, and in comparison with the electron density within the 12MR channel of the pure mordenite.

Soft constraints were imposed on tetrahedral bond lengths Si–O (1.605 Å) as well as on the C–C (1.38 Å), C–Cl (1.72 Å), S–C (1.73 Å), N–N (1.35 Å), and S–N (1.65 Å) distances with tolerance values (σ) of 0.002. The weight on these constraints could not be removed without unrealistic bond distances emerging in the structure, and was therefore kept at a value of 500 in the last cycles of the refinement. The population of individual atoms and isotropic displacement factors were constrained to be equal for sulfachloropyridazine molecules. The crystallographic data and refinement details are reported in Table 2.

The final atomic positions and thermal parameters are given as supporting information in Table 1S. Final observed and calculated powder pattern of HS-MOR/SC is shown as supporting information as well in Fig. 1S.

2.5. Adsorption kinetics

Mordenite was added to sulfachloropyridazine solutions (ca. 40 µM each) with a zeolite:antibiotic aqueous solution ratio of 1 mg:2 mL in polyallomer centrifuge tubes (Nalgene, New York, USA). Suspensions were shaken for different time intervals and then centrifuged at 20,000g for 15 min. The supernatant was withdrawn and analysed by HPLC. The amount of antibiotic adsorbed by zeolite was calculated by the difference between the initial and final concentrations. Kinetics was performed in triplicate at both RT and 65 °C. Controls were run at the same temperatures in the absence of mordenite in order to check the stability of the sulfachloropyridazine and if the antibiotic adsorbs on the centrifuge tube walls. No decrease in its concentration was recorded in the controls for the entire duration of the experiment.

2.6. Adsorption–desorption isotherms

Sulfachloropyridazine adsorption isotherm on zeolite was performed in distilled water at RT with a zeolite:antibiotic solution ratio of 1 mg:2 mL. Zeolite was exposed to a number of adsorption cycles in the presence of the antibiotic solution at maximal solubility, owing to the low solubility of sulfachloropyridazine and to the high adsorption capacity of mordenite. At each adsorption cycle, the suspension was shaken for 6 h and then centrifuged. The supernatant was therefore removed and analysed by HPLC, and replaced by fresh sulfachloropyridazine solution. Subsequent adsorption cycles were performed until mordenite reached its maximal adsorption capacity (exhausted zeolite). Adsorption experiments were conducted in triplicate.

The antibiotic concentration in aqueous phase at equilibrium was expressed as C_e (µM) whereas the amount of antibiotics adsorbed in zeolite was calculated by the difference between the initial and final (C_e) concentrations and expressed as C_s (µmol g^{-1} adsorbent).

In a separate experiment, the exhausted zeolite suspension with the remaining antibiotic solution after the last adsorption cycle was used to test the antibiotic desorption: isotherms were carried out on exhausted zeolite by following the dilution technique as follows. One-half volume of supernatant containing the antibiotic was removed and substituted with distilled water. The system was then shaken for 6 h and centrifuged. Then, a second half-volume of the diluted supernatant was replaced by an equal volume of distilled water and analysed. The dilution step was repeated three times. The chemical concentration after each desorption step

Table 2
Lattice parameters and refinement details for mordenite before and after sulfachloropyridazine adsorption.

	HS-MOR	HS-MOR/SC
Space group	Orthorhombic, $Cmc2_1$	Orthorhombic, $Cmc2_1$
a (Å)	18.0660(5)	18.0696(6)
b (Å)	20.2148(6)	20.2338(5)
c (Å)	7.4538(2)	7.4560(2)
$\alpha = \beta = \gamma°$	90	90
V (Å^3)	2722.2(1)	2726.0(1)
Wavelength of incident radiation (Å)	1.5417(1)	1.5417(1)
Refined pattern 2θ range (°)	3–116	4–116
Profile function	T-C-H pseudo-Voigt correction	T-C-H pseudo-Voigt correction
H-atom treatment	Not refined	Not refined
R_{wp} (%)	11.3	12.0
R_p (%)	9.2	9.4
R_F^2 (%)	6.3	10.4
N_o of contributing reflections	5673	5690
N_{obs}	2336	2256
N_{var}	114	117

$R_p = \sum [Y_{io} - Y_{ic}] / \sum Y_{io}$; $R_{wp} = [\sum W_i (Y_{io} - Y_{ic})^2 / \sum W_i Y_{io}^2]^{0.5}$; $R_F^2 = \sum |F_o^2 - F_c^2| / \sum F_o^2$; Estimated standard deviations in parentheses refer to the last digit.

(C_e) was determined using HPLC, and the amount which remained adsorbed in the zeolite (C_s) was calculated by the difference. Desorption experiments were conducted in triplicate.

2.7. FTIR spectroscopy

Infrared spectra were collected on a Thermo Electron Corporation FT Nicolet 5700 Spectrometer with 4 cm^{-1} resolution. Self-supporting pellets of mordenite bare and loaded with sulfachloropyridazine were obtained with a mechanical press at ca. 7 tons cm^{-2} and placed into an IR cell equipped with KBr windows permanently attached to a vacuum line (residual pressure: $\leqslant 1 \times 10^{-4}$ Torr), allowing all treatments to be carried out in situ. Air-dried HS-MOR/SC samples were outgassed at RT for 30 min in order to remove adsorbed water before FTIR analysis. FTIR spectra of sulfachloropyridazine in CH_2Cl_2 solution were performed in a standard KBr cell for liquids.

The IR spectrum of the sulfachloropyridazine reaction product was not recorded owing to its very scarce solubility into CH_2Cl_2 and $CHCl_3$.

2.8. Chromatographic analyses

The concentration of the sulfachloropyridazine was determined by HPLC–UV. The system was assembled with a Jasco 880-PU Intelligent pump, a Jasco AS-2055 plus Intelligent Sampler, a Jasco 875-UV Intelligent DAD detector at 270 nm, Borwin v 1.2160 chromatography software, a Jones Chromatography model 7971 column heater, and a 4.60 mm × 150 mm Synergi 4 µm Hydro-RP 80A analytical column (Phenomenex, USA). The analytical column was kept at 35 °C and eluted with acetonitrile:water (20:80 by volume, pH 2.7 for H_3PO_4) eluant at 1 mL min^{-1} flow. All solvents were HPLC grade. Under these chromatographic conditions, the retention times for sulfachloropyridazine and its degradation product (λ_{max} 270 nm) were 8.6 min and 2.7 min, respectively.

2.9. Isolation of sulfachloropyridazine reaction product

Monitoring by HPLC the supernatant of the mordenite-antibiotic suspension kept at 65 °C, a single sulfachloropyridazine reaction product appeared contemporaneously to the antibiotic disappearance. As several milligrams of by-product were needed for its identification, a suspension of 1 L of antibiotic solution at maximal solubility containing 500 mg HS-MOR was stirred at 65 °C in the dark for three weeks and after that, the suspension was centrifuged and the supernatant concentrated by evaporation at 65 °C. After centrifugation, mordenite was washed with methanol in order to recover possibly adsorbed transformation product but only sulfachloropyridazine was detected.

As the initial pH of mordenite-antibiotic suspension was 4.0, an aqueous solution of sulfachloropyridazine was kept at the same pH and 65 °C in the dark for three weeks as control. Also an antibiotic solution at pH 10 was tested to produce high yield of antibiotic reaction product.

The reaction product was isolated, as a white crystal, by liquid chromatography on silica gel (Kiesel Gel 60, 70–230 mesh, Macherey–Nagel, Germany) using a mixture of hexane and ethyl acetate (20:80 = v:v) followed by pure ethyl acetate as eluant.

2.10. Identification of sulfachloropyridazine reaction product

2.10.1. GC–MS

The mass analysis of the sulfachloropyridazine transformation product was carried out by HPLC–MS (Agilent Technologies 1100 series equipped with DAD detector, binary pump, autosampler and interfaced with electrospray source ESI-MS), the product was injected onto a reversed phase LC column (Phenomenex Gemini C18 100 × 3.00 mm, 3 m, 110 Å) eluted at a flow rate of 0.4 mL min^{-1}. The mobile phases were: A (water – mQ ultra pure 18.6 MΩ cm) and B (acetonitrile CHROMOSOLV HPLC grade Sigma–Aldrich), both containing 0.1% formic acid. A linear gradient elution was performed from 30% to 80% of solvent B over 8 min, 80% of B until 22 min, from 80% to 90% over 24 min. The ESI source was operated under the following conditions: capillary voltage 4500 V, drying gas flow 12.5 L min^{-1}, nebulizer pressure 30 psi, drying gas temperature 350 °C. The ions were scanned in positive full mode over m/z 100–2600, scan time 0.1 s. Under these LC–MS conditions, the retention time of the transformation product was 4.82 min with m/z (%): 267 (75) [M+H]$^+$, 289 (100) [M+Na]$^+$.

2.10.2. NMR

One and bidimensional NMR spectra were obtained at 400 MHz and 25 °C using a Varian Mercury plus spectrometer. One-dimensional ^1H spectra were recorded using the following parameters: pw = 6.3 µs (90°), sw = 4000 Hz, d1 = 2 s, np = 16 K and Fourier-transformed to 64 K with lb = 0.5. Two-dimensional gHSQC and gHMBC spectra were recorded using library sequences with the following parameters sw = 4000 Hz, sw1 = 20121 Hz (gHSQC) or
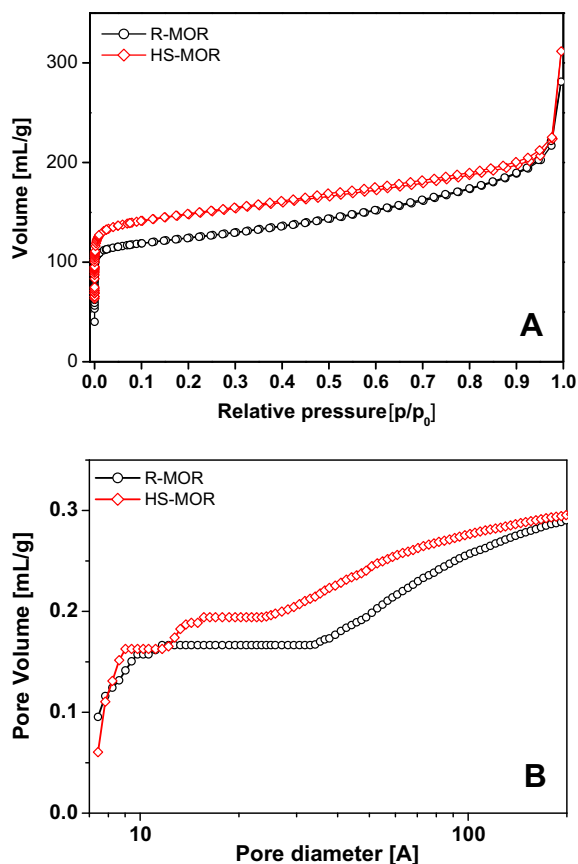
Fig. 1. N_2 physisorption isotherms (A) and plots of cumulative pore volume *vs* pore diameter (B) for high silica mordenite (HS-MOR, $SiO_2/Al_2O_3 = 200$), and reference sample (R-MOR, $SiO_2/Al_2O_3 = 20$).

Table 3
Specific surface area and pore volume determined by N_2 physisorption measurements and applying the Brunauer–Emmet–Teller (BET) and non-local density functional theory (NLDFT) methods, respectively.

Samples	R-MOR	HS-MOR
SiO_2/Al_2O_3	20	200
BET surface area ($m^2 g^{-1}$)	386	453
Micropore area ($m^2 g^{-1}$)[a]	261	278
External surface area ($m^2 g^{-1}$)[a]	125	175
Total pore volume (mL g^{-1})	0.258	0.277
Micropore volume (mL g^{-1})[b]	0.167	0.194
Mesopore Volume (mL g^{-1})[c]	0.091	0.083

[a] Determined by *t*-plot method.
[b] Pores up to 20 Å.
[c] Pores in the range 20–100 Å.

sw1 = 26152 (gHMBC), np = 2048, ni = 128 and Fourier-transformed to 4096 (f2) and 2048 (f1) points after Gaussian apodisation in both dimensions. One-bond J_{CH} was set to 140 Hz for gHSQC and gHMBC. Multiple bond J_{CH} was set to 8 Hz for gHMBC.

3. Results and discussion

The crystal structure of sulfachloropyridazine reported in Table 1 was determined by single-crystal X ray diffraction by Tan et al. [29] and shows a distorted bended configuration, with the pyridazine and benzene rings forming a dihedral angle of 82.86(6)°. The molecular dimensions of sulfachloropyridazine (Table 1) are compatible with the opening of the mordenite zeolite

pore system, thus making its diffusion through the 12MR channel possible. This tight fit limits rotational disorder within the channel and simplifies the accurate localization of the molecule and the characterization of molecule-framework interactions.

3.1. Characterization of mordenite

3.1.1. Surface area and porosimetric analysis

N_2 adsorption isotherms (Fig. 1A) show a high uptake at relative pressure lower than 0.05 because of micropore filling, which is significantly higher for the high silica mordenite (HS-MOR, $SiO_2/Al_2O_3 = 200$), in comparison to the reference sample (R-MOR, $SiO_2/Al_2O_3 = 20$). The specific surface area of HS-MOR determined by the Brunauer–Emmett–Teller (BET) approach is 453 $m^2 g^{-1}$, most of which related to the presence of micropores (278 $m^2 g^{-1}$) (Table 3). Both these values are higher than those of the R-MOR sample, 386 and 261 $m^2 g^{-1}$ respectively. In agreement to this, the cumulative micropore volume (pores up to 20 Å) of the HS-MOR sample, 0.194 mL g^{-1}, determined by NLDFT method and using a cylindrical pore model, is higher than that of R-MOR, 0.167 mL g^{-1} (Table 3 and Fig. 1B): this is a clear effect of the dealumination process that produces defects in the HS-MOR structure, and leads to an enlargement of both the main channels and the side pockets [1,3]. Finally, both samples have a significant fraction of mesopores (pore diameter in the 20–100 Å range) due to particles aggregation.

3.1.2. Thermogravimetric analysis

To study the defectivity (i.e. silanols concentration) and hydrophobicity of the mordenite samples selected for this study, thermogravimetric analysis (TGA) has been performed (Fig. 2).

TGA of the reference mordenite (R-MOR) in protonic form shows in the 30–350 °C range a considerable weight loss (11.4% zeolite weight, curve a). In this region an asymmetric profile for the related derivative curve (curve a′) reveals the presence of several type of adsorbed water. The derivative signal can be resolved in three components at ca. 100, 150, and 220 °C due to the loss of physisorbed water, water belonging to solvation sphere of protons and water bound to either protons or aluminium atoms, respectively. Over 350 °C the weight loss is almost negligible.

The weight loss of HS-MOR (curve b) between 30 and 350 °C (5.3% zeolite DW) is significantly lower than what found for R-MOR. Two zones can be distinguished in the 30–800 °C range: the first between 30 and 170 °C with a steeper weight loss (ca. 4.7% zeolite dried weight - DW), due to water adsorbed into the zeolite pores, and the second between 170 and 800 °C with a more gradual loss accounting for additional 1.7% zeolite DW due to the condensation of silanol groups, which were clearly detected by IR spectroscopy (*vide infra*). The derivative curve (Fig. 2, curve b′) in the first temperature range shows a signal sharper than for R-MOR due to the absence of water bound to protons and aluminium atoms. On the basis of the water loss of the two selected mordenite types, it can be inferred that HS-MOR is less hydrophilic than R-MOR and contains a significant amount of silanols: considering the water loss due to silanol condensation, 4 silanol groups per unitary cell of HS-MOR are found by TGA, in broad agreement with results of Refs. [1,4]. Assuming that four silanol groups are generated by extracting a single T atom, the unit cell is described by the formula:

$$T_{47}O_{92}(OH)_4.$$
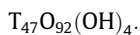
3.2. Adsorption kinetics

The adsorption kinetics of sulfachloropyridazine into HS-MOR has been performed in order to define the adsorption time needed
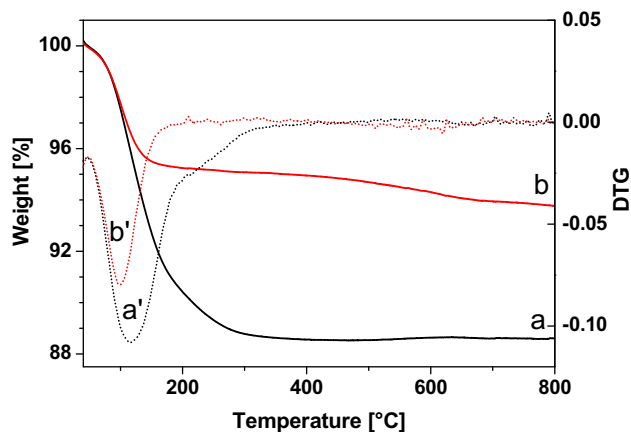
Fig. 2. Thermogravimetric analysis of reference mordenite ($SiO_2/Al_2O_3 = 20$, curve a) and high silica mordenite ($SiO_2/Al_2O_3 = 200$, curve b) in dry air atmosphere; the derivative profiles (DTG) for both samples are also reported (curves a′ and b′, respectively).
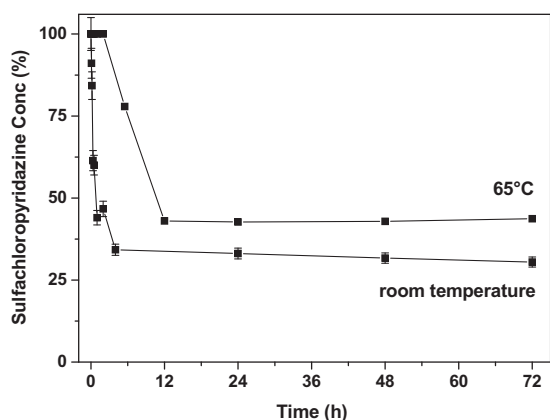

Fig. 3. Adsorption kinetics of sulfachloropyridazine (40 μM) into high silica mordenite (antibiotic solution:zeolite = 2 mL:1 mg) at different temperatures. SD as vertical bars. When not visible, SD bar is within the symbol dimension. The adsorption equilibrium is reached in 4 h.

for sulfachloropyridazine to reach the adsorption equilibrium. As shown in Fig. 3, at RT ca. 70% of sulfachloropyridazine initial amount was retained by mordenite already after 4 h and no significant variations have been recorded subsequently.

Therefore, the adsorption at RT in the subsequent trials was performed with a contact time slightly higher (6 h) to permit the process to largely reach the equilibrium state.

In a previous work conducted by some of the present authors, the adsorption of sulfachloropyridazine in faujasite Y with 200 SiO_2/Al_2O_3 showed a more favourable adsorption kinetics with less than 1 min as equilibrium time [7]. The difference in adsorption kinetics between faujasite and mordenite can be due to the different structural conformation of the two sorbents: firstly, the access window in mordenite has dimensions slightly smaller than in faujasite (7.0 Å × 6.5 Å *vs* 7.0 Å × 7.1 Å); secondly, the parallel linear channels occurring in mordenite may limit the diffusion of the antibiotic molecule if compared to the interconnected supercages system of faujasite.

In mordenite the effect of temperature on the antibiotic adsorption was investigated repeating the kinetics at higher temperature. Conversely to what observed at RT, at 65 °C the adsorption equilibrium was reached by 12 h contact time when the adsorbed sulfa-

chloropyridazine attested at ca. 55% of the initial amount: the adsorption was less pronounced than what it was found at RT since the adsorption is an exothermic process.

3.3. Adsorption/desorption isotherms

The sulfachloropyridazine aqueous solutions used for the adsorption experiments were prepared at concentration ca. 1 order of magnitude higher than those measured in effluents from fish feedings according to the National Aquaculture Association (2003) and ca. 3 orders higher than their occurrence in natural waters [30,31]. This procedure was considered opportune for obtaining the maximal loadings of zeolite in the shortest time to subsequently perform thermogravimetric, spectroscopic and diffractometric analyses of exhausted air-dried zeolite.

In order to define the affinity of sulfachloropyridazine for mordenite and the maximal adsorption capacity of the zeolite, the adsorption isotherm was performed and the amount of antibiotic remained in the solution at the equilibrium point (C_{eq}), after each adsorption cycle, was reported (Fig. 4) as a function of the antibiotic adsorbed in HS-MOR zeolite (C_s).

The adsorption isotherm clearly shows a two-stage trend: the first one is represented by the isotherm segment at low sulfa drug concentration (ranging from 0 to ca. 270 μmol g^{-1} zeolite DW along C_s axis); the second one is described by the isotherm segment at higher concentrations. In the absence of degradation products, as in this case, these features could describe the different affinity of sulfonamide for zeolite adsorption sites. This different affinity was hypothesised as due to interaction with different adsorption sites. It is likely that once the sites at higher affinity are completely involved in the antibiotic retention, adsorption continues on the sites at lower affinity. As elucidated in the following part of the paper, the sites at different affinity can be identified as silanol and siloxane groups located at both external and internal zeolite surfaces. The overall migration of antibiotic on adsorption sites continued till the process arrested at ca. 530 μmol g^{-1} zeolite DW, accounting for 15.1% mordenite DW. The amount of sulfachloropyridazine on exhausted zeolite determined by TGA attested at 12.3% zeolite DW (Fig. 2S as supporting information). Although the two loading values are not very close, they are both acceptable in the light of the very different experimental techniques used. Considering the loading determined by HPLC and taking into account both silanol and sulfonamide concentration, the following unit cell compositions can be defined:

$$\left[T_{47}O_{92}(OH)_4 \; SC_{1.8} \right]$$
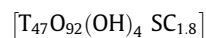
The high drug loading is likely due to the fact that, at the pH of the antibiotic/zeolite suspension (ca. 4), the most abundant species for sulfachloropyridazine is the neutral form (according to its pKa = 5.5). In fact, as already proved by Fukahori et al. on high silica zeolite Y, the most absorbable form of sulfa drugs was the neutral one.

The reversibility of the adsorption process was evaluated by performing desorption experiments on exhausted zeolites by diluting the antibiotic concentration at the equilibrium point. As reported in Fig. 4, the desorption process did not have any significant effect on the release of the antibiotics from the zeolite. In fact, in case of adsorption reversibility, the desorption isotherm derived from data points obtained at each desorption step should overlap the adsorption curve. On the contrary, according to our data, the desorption curve is almost parallel to the *x* axis, revealing the tendency of the drug to remain entrapped inside the zeolite channels/pores. These findings are indicative of an irreversible adsorption process.
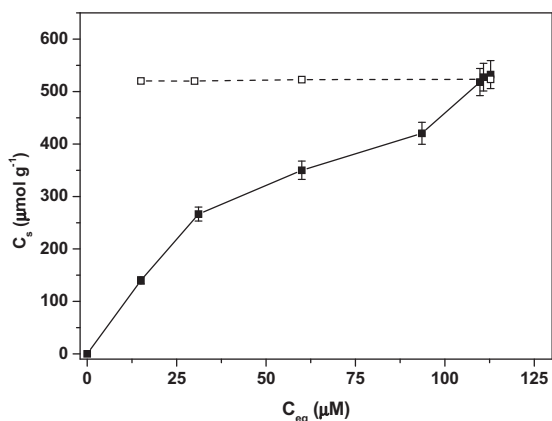
Fig. 4. Adsorption (solid squares) and desorption (open squares) isotherms of sulfachloropyridazine into high silica mordenite (antibiotic solution:zeolite = 2 mL:1 mg) at RT and 6 h contact time. SD as vertical bars. The maximal antibiotic loading was about 530 μmol g^{-1} zeolite dry weight (15.1 wt.%).

3.4. Rietveld refinement

The question now arises: where are sulfachloropyridazine molecules located inside the porous structure? To answer this question, X-ray powder diffraction (XRPD) analyses were performed. The comparison of the XRPD patterns of as-received HS-MOR and the sample after sulfachloropyridazine adsorption (HS-MOR/SC) shows strong differences in the intensity of diffraction peaks in all 2θ range investigated (Fig. 5).

The most significant effect is a decrease in intensities at low 2θ angles, which is typical of increased disorder in the extraframework sites and suggests that the two samples have a different extraframework content and, consequently, different atomic parameters (such as positional coordinates x, y, z, isotropic temperature factor, and occupancies). The positions of diffraction peaks

(which strongly depend on cell parameters values, Table 2) in the two patterns are only slightly different. All these features clearly indicate that the mordenite crystal structure was modified by the antibiotic adsorption.

In the present study, any attempt to refine positions and displacement parameters over the complete 2θ range starting from the framework atoms of HS-MOR (C*mcm* space group [9]) was not satisfactory because of poor agreement factors for the whole pattern. The quality of Rietveld structure refinement was strongly improved in the C*mc*2$_1$ space group, a subgroup of C*mcm*. The symmetry reduction from centric C*mcm* to acentric C*mc*2$_1$ was justified by the deviation of the T-O11-T angle (172.8°, corresponding to T-O8-T angle in the C*mcm* space group) from the unfavourable 180° value imposed by the topological symmetry. This result increases the possibility for O11 oxygens to occupy different sites and, consequently, to undergo a symmetry reduction from orthorhombic to monoclinic. Unfortunately, the quality of our data does not allow us to have direct experimental evidence for the monoclinic symmetry and, consequently, the C*mc*2$_1$ space group was maintained in our structure refinement. Strong deviation of T-O11-T angle from 180° (170°), was also observed in the as-received material thus suggesting that the most probable real symmetry in both HS-MOR and HS-MOR/SC samples is lower than the topological one (probably orthorhombic C*mc*2$_1$ or lower). Symmetry lowering from the highest symmetry C*mcm* are also reported in natural, synthetic and H-mordenite [9–10,27,32], depending on the extraframework cation content, the Si/Al ordering, and the hydration/dehydration level [33–36].

Rietveld refinement of unit cell parameters of HS-MOR/SC sample reveals small variations in comparison to those of the HS-MOR material (Table 2). This confirms that the drug is included in the zeolite microporosity which, to some extent, reflects on the geometry of zeolite channels (Fig. 6).

An enlargement of the 12MR channel occurs as a consequence of the embedded antibiotic, and the Crystallographic Free Area (C.F.A.) (*sensu* [37]) changes from more elliptical (36.04 Å^3 C.F.A.
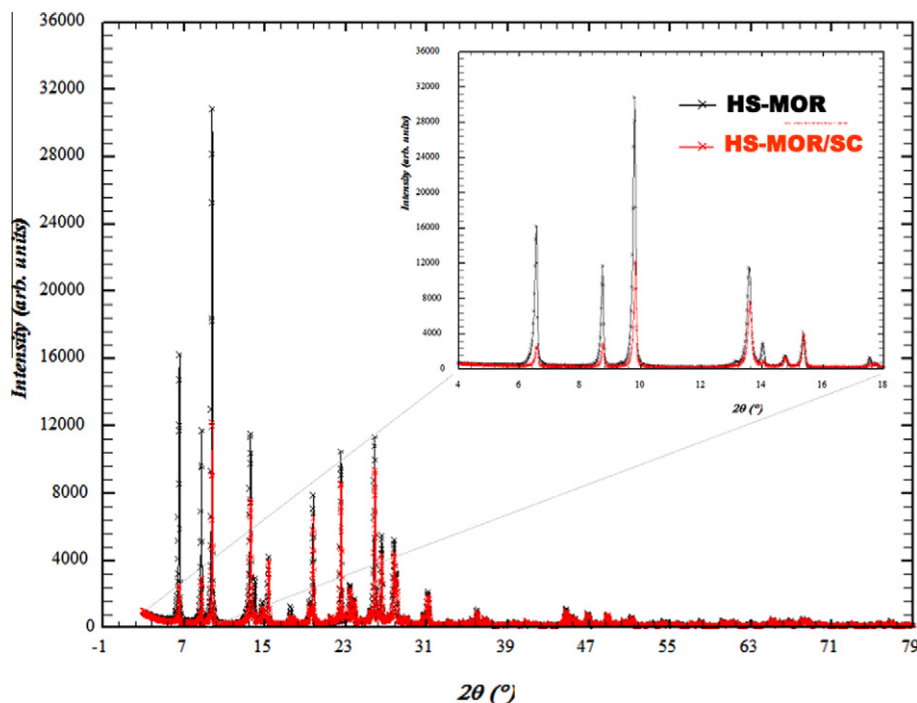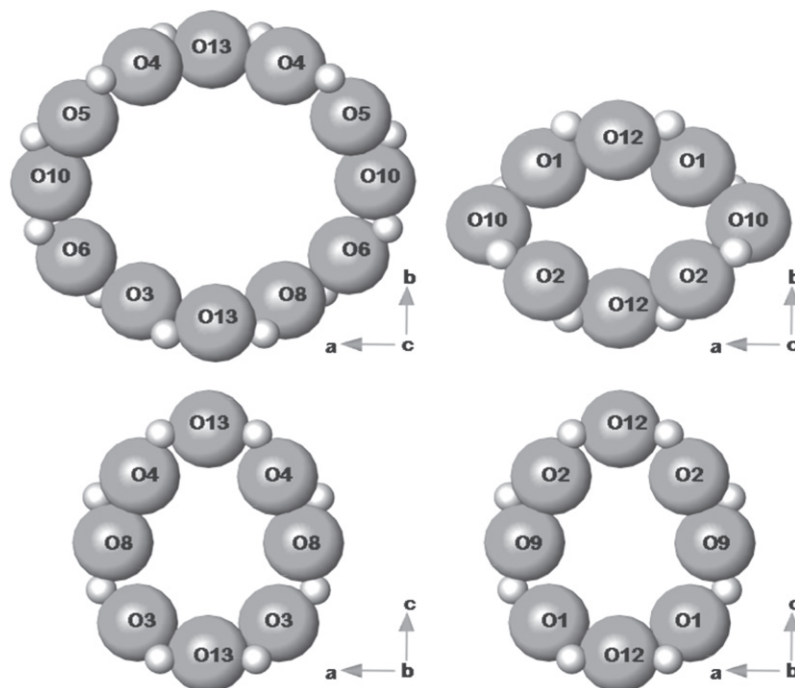

Fig. 5. Observed X-ray powder diffraction patterns of bare mordenite (HS-MOR: black curve) and sulfachloropyridazine loaded mordenite (HS-MOR/SC: red curve). (For interpretation of the references to colour in this figure legend, the reader is referred to the web version of this article.)

12MR [001]	C.F.A.*	O13-O13	O3-O4	O10-O10	O5-O6
HS-MOR	36.04	8.76(1)	9.12(1)	10.06(1)	9.90(1)
HS-MOR/SC	36.78	8.98(1)	9.13(1)	10.05(1)	9.99(1)
8MR [001]	C.F.A.*	O12-O12	O2-O1	O10-O10	
HS-MOR	10.41	5.68(1)	5.84(1)	8.01(1)	
HS-MOR/SC	10.19	5.41(1)	5.89(1)	8.02(1)	
Side Pocket 8MR [001]	C.F.A.*	O12-O12	O2-O1	O9-O9	
HS-MOR	11.80	7.45(1)	6.34(1)	6.18(1)	
HS-MOR/SC	12.69	7.46(1)	6.62(1)	6.18(1)	
Side Pocket 8MR [001]	C.F.A.*	O13-O13	O4-O3	O8-O8	
HS-MOR	12.91	7.45(1)	6.71(1)	6.15(1)	
HS-MOR/SC	13.02	7.46(1)	6.62(1)	6.39(1)	

* Crystallographic Free Area calculated using for the ring diameter the mean of the O-O distances reported in the Table.

Fig. 6. Crystallographic Free Area (C.F.A.) and dimensions (Å) of the mordenite apertures before (HS-MOR) and after sulfachloropyridazine adsorption (HS-MOR/SC); an oxygen ionic radius of 1.35 Å is assumed.

in HS-MOR) to a nearly circular form (36.78 Å^3 in HS-MOR/SC). The distortion of the 12MR channel was accompanied by deformations of the 8MR ring (C.F.A. = 10.41 and 10.19 Å^3 in HS-MOR and HS-MOR/SC, respectively, Fig. 6). An analogous distortion mechanism was also observed in the 8MR of the side pocket, which increases their C.F.A. after sulfachloropyridazine adsorption. The combined effect of widening/contraction of both channel systems justifies the small variations in the unit cell parameters reported in Table 2.

The difference Fourier map generated using the GSAS package, revealed the presence of ten extraframework sites (Table 1S in supporting information), which were attributed to atoms of encapsulated sulfachloropyridazine molecules. Moreover, using this assumption, reasonable values were obtained for C–C, C–N, S–O,

N–Cl and C–Cl bond distances in the antibiotic molecule, comparable to those found in free antibiotic [29]. The geometry of sulfachloropyridazine molecule, as well as the very similar occupancy values and isotropic displacement parameters obtained for the extraframework atoms, confirmed that the observed peaks had been correctly attributed to the antibiotic molecule.

Rietveld structure refinement revealed the presence of about 1.5 antibiotic molecules per unit cell, in good agreement with the maximal adsorption capacity determined by the adsorption isotherm (Fig. 4, $[Si_{47}O_{92}(OH)_4]$ $SC_{1.8}$). These molecules show two different orientations due to the presence of the screw axis parallel to [001] and lie in the large 12MR channel, with the pyridazine ring (C1, C2, C3, and C4 atoms, respectively) oriented towards the
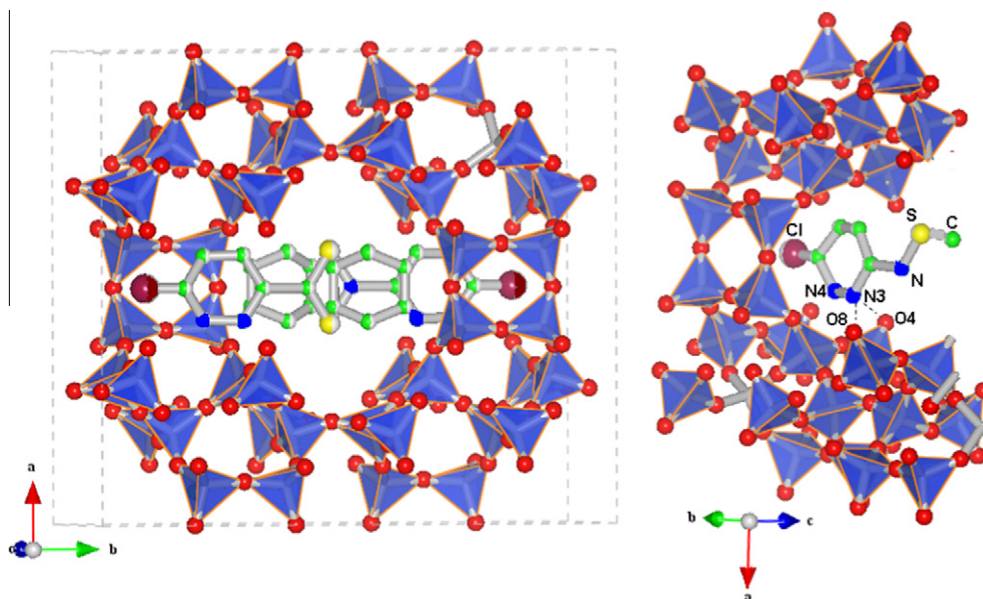
Fig. 7. Mordenite-sulfachloropyridazine adduct projection along [0 0 1] (left side) showing the drug (Cl represented with brown, C with green, N with blue, and S with yellow, respectively). On the right side, the location of pyridazine ring with respect to framework oxygens of mordenite side pocket is shown.
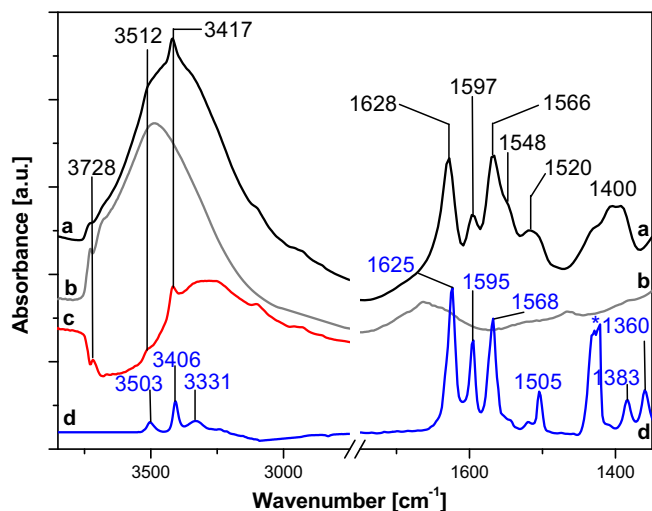

Fig. 8. Infrared spectra of sulfachloropyridazine adsorbed into high silica mordenite (a). Spectrum of bare mordenite is reported for comparison (b). Curve c refers to the difference spectrum of the drug adsorbed into mordenite obtained by subtracting curve b to a. Spectrum of sulfachloropyridazine in CH_2Cl_2 is also reported (d): asterisk indicates a band whose shape and intensity cannot be recorded with precision because strongly overlapped to the most intense CH_2Cl_2 band at 1430 cm^{-1}.

mordenite channel side pocket and parallel to the *b* direction (Fig. 7).

The pyridazine and aniline rings (C5, C6, and C7 atoms, respectively) form a bended configuration indicated by the torsion angle S–N–C2 of about 130°, which is larger than in sulfachloropyridazine (126.6° [26]). The aniline ring protrudes towards the 12MR channel centre. The positions occupied by nitrogen atoms of the pyridazine ring, as well as by oxygen atoms bound to the sulphur, appear strongly disordered and consequently are not localised. The presence of the mirror plane orthogonal to [1 0 0] imposes that in pyridazine ring C3 and C4 sites can host either C or N atoms. This result confirms that, owing to the position of sulfachloropyridazine

molecule, the most probable real symmetry of HS-MOR/SC is lower than $Cmc2_1$.

The refined distances of pyridazine ring atoms with the framework oxygens (C3/N3–O4 = 2.12(7) Å, C3/N3–O8 = 2.06(8) Å, C4/N4–O4 = 2.43(6) Å, C4/N4–O8 = 2.44(6) Å, respectively) indicate that these species are capable to give H-bonds with nitrogen atoms of the antibiotic pyridazine ring as clearly demonstrated by IR analysis (*vide infra* Fig. 8). Notwithstanding the refined interatomic bond distances are affected by the uncertainty in powder refinements (many studies have indicated that a more realistic estimate of the uncertainties in the results is obtained if the estimated standard deviations are multiplied by a factor of about 3 [38]), our results strongly suggest that silanol groups exist at the intersection between 12MR and 8MR channels.

The presence of strong interaction between guest organic molecules and framework oxygen atoms, was also recently reported in the same high silica mordenite after carbamazepine [6], levofloxacin [6], 1,2-dichloroethane [9], methyl *tert*-butyl ether, and toluene adsorption [10]. Also in all these cases, the incorporation of organic molecules caused a remarkable change in the dimension of both 8MR and 12MR rings, when compared to the parent zeolite. As a consequence, the ellipticity (ε) (defined as the ratio between the larger (O–O) and smaller (O–O) "free diameters") of both apertures changes after organic molecules adsorption, thus indicating a framework flexibility of mordenite (Table 4).

3.5. FTIR

The host–guest interactions between sulfachloropyridazine and mordenite responsible for the irreversible adsorption from water were elucidated by means of infrared spectroscopy. In Fig. 8, the IR spectrum of antibiotic adsorbed into zeolite at the maximal loading is shown (curve a) along with the spectra of bare mordenite (curve b) and the difference curve between spectra a and b (curve c). Pure drug in CH_2Cl_2 (curve d) is also reported. Both samples have been outgassed before the spectroscopic analysis to remove water adsorbed on zeolite surfaces.

The spectrum of bare mordenite shows a complex and intense band in the region between 3750 and 3000 cm^{-1} where silanol

Table 4
Ellipticity of the apertures in HS-MOR zeolite before and after sulfachloropyridazine adsorption. Crystallographic Free Areas (C.F.A.) *sensu* Baerlocher [37] are also reported.

12MR [001]	C.F.A.	Ellipticity	8MR [001]	C.F.A.	Ellipticity	References
HS-MOR	36.04	1.148	HS-MOR	10.41	1.410	This work
HS-MOR/SC	36.78	1.119	HS-MOR/SC	10.19	1.482	This work
DCE-MOR	35.90	1.169	DCE-MOR	10.40	1.425	[9]
MTBE-MOR	34.31	1.138	MTBE-MOR	10.12	1.500	[10]
TOL-MOR	36.63	1.141	TOL-MOR	9.98	1.573	[10]
CBZ-MOR	32.00	1.219	CBZ-MOR	10.03	1.445	[6]
FLX-MOR	33.22	1.165	FLX-MOR	10.83	1.415	[6]

DCE: dichlorethane; MTBE: Methyl *tert*-butyl ether; TOL: toluene; CBZ: carbamazepine; FLX: levofloxacin.
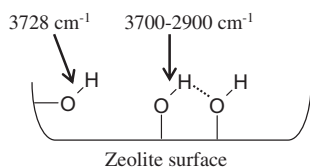
Scheme 1. Schematic representation of isolated (left) and H-bond donor silanols (right) on zeolite surface.
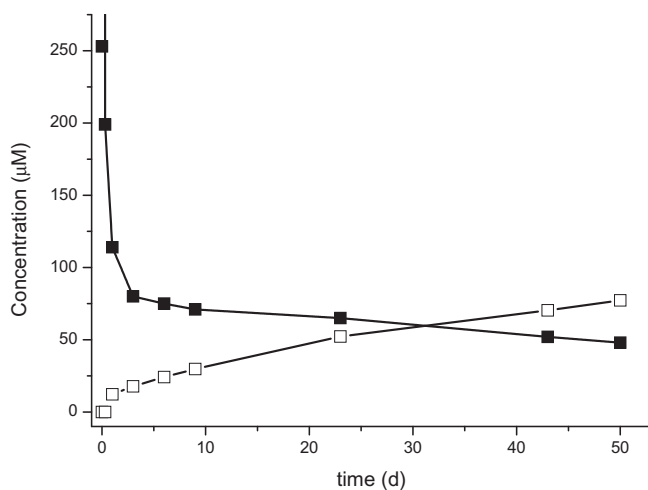
Fig. 9. Sulfachloropyridazine antibiotic (full squares) and its reaction product (open squares) concentration in the aqueous solution at 65 °C in contact with high silica mordenite.

groups absorb [39]. This high intensity is attributable to the large amount of silanol defects produced by the dealumination process [1,4]. A defined and weak band due to isolated silanols inside micoporosities is found at 3728 cm^{-1} whereas the most intense and broad band in the range 3700–2900 cm^{-1} is assigned to H-bonded donor (i.e. vicinal) silanols (Scheme 1) [39,40].

After antibiotic adsorption (Fig. 8, curve a), the band at 3728 cm^{-1} almost completely disappears whereas the intense band of H-bonded silanols is downshifted and enlarged at the same time. These findings indicate that a significant fraction of silanols are bound to the antibiotic. Moreover, bands of the antibiotic at 3417 cm^{-1} (sharp) and in the range 3250–2750 cm^{-1} (very weak), which are overlapped to the broad absorption of silanol groups, can be clearly identified.

To better visualise the silanol fraction involved in the interaction with sulfachloropyridazine, a difference spectrum of the mordenite before (curve b) and after the drug adsorption has been reported (curve c): it is clear that a significant portion of the band of silanols is eroded after antibiotic adsorption (negative band in the range 3750–3400 cm^{-1}) and a new band is formed at lower frequencies (positive band in the range 3400–3000 cm^{-1} whose maximum is found at ca. 3300 cm^{-1}). This is a clear-cut evidence of the fact that H-bonding interactions of medium strength [41] occur between silanols and sulfachloropyridazine. The difference curve shows that not only isolated silanols interact with the drug but H-bonded vicinal silanols are also capable to bind the antibiotic molecule.

The IR bands of antibiotic in CH$_2$Cl$_2$ (curve d) have been already assigned comparing the observed absorptions with the theoretical frequencies computed for the isolated molecule [8]. The asymmetric and symmetric stretching modes of amino group in pure antibiotic absorb at 3503 and 3406 cm^{-1}, respectively. In the silanol-drug adduct (spectrum a), only the symmetric stretching at 3417 cm^{-1} is clearly visible. The weak band of asymmetric stretching of amino group can be found in the difference spectrum (curve c) as a shoulder at 3512 cm^{-1}. If compared to the spectrum of antibiotic in CH$_2$Cl$_2$, the upshifted stretching modes for the amino group of the adsorbed drug clearly indicate that this group experiences an environment less polar than CH$_2$Cl$_2$, thus ruling out the involvement of the amino group in the formation of H-bonding with the zeolite silanols. This is in full agreement with the structure determined by XRPD Refinement analysis (Fig. 7).

In pure sulfachloropyridazine, the weak band at 3331 cm^{-1} is assigned to the stretching mode of sulfonamide amidic group [8]. Unfortunately, this absorption is not clearly measurable once the drug is adsorbed into mordenite because overlapped to the intense and broad band of zeolite silanols.

In the spectrum of pure antibiotic, the bands at 1625 and 1595 cm^{-1} are respectively assigned to the amino group bending vibration and to the phenyl ring quadrant stretching coupled with the amino group bending mode [8]. In the adsorbed molecule, these modes are almost unchanged in terms of both wavenumber (1628 and 1597 cm^{-1}, respectively) and relative intensity, thus suggesting only small perturbation of the aniline ring upon adsorption. Again, this is consistent with the fact that the aniline ring is found protruding toward the zeolite channel centre as shown in Fig. 7 by the Rietveld analysis.

The band at 1568 cm^{-1}, which is assigned in pure antibiotic to the coupling of quadrant stretching modes of both phenyl and pyridazinyl rings, it is found in similar position for the adsorbed drug. A shoulder at 1548 cm^{-1} is found for the adsorbed antibiotic (curve a): this absorption was also found in the spectrum of the drug adsorbed into high silica zeolite Y and is assigned to the heterocycle quadrant stretching coupled with the NH bending [8].

The spectrum of the adsorbed drug at frequency lower that 1530 cm^{-1} is very different to that of the molecule in solution. This is not surprising as in this region essentially fall collective modes of the pyridazine ring, which is H-bonded to the mordenite internal silanols (see Rietveld analysis results in Fig. 7), and therefore a significant perturbation of the molecular and electronic structure of the heterocyclic ring is expected.

Table 5

^{1}H and ^{13}C NMR chemical shift of sulfachloropyridazine reaction product (X = OH, 4-amino-*N*-(6-hydroxyl-3-pyridazinyl)benzene sulfonamide) and SC (X = Cl) in CD$_3$OD. Atom numbering is given according to the ACD/ChemSketch 12.0 program and indicated in the scheme below.

Atom number	Reaction product		Sulfachloropyridazine	
	^{1}H	^{13}C	^{1}H	^{13}C
1	–	–		
2	–	–		
3	–	144.9	–	156.2
4	7.50	131.8	7.63	122.6
5	6.95	133.0	7.62	132.2
6	–	162.8	–	152.2
7	10.57*	–	11.65*	–
8	–	–		
9	–	127.5		127.5
10/14	7.56	130.9	7.65	130.7
11/13	6.67	114.8	6.67	114.4
12	–	155.3		155.3
15	12.36*	–	–	
16	5.99*	–	6.11*	
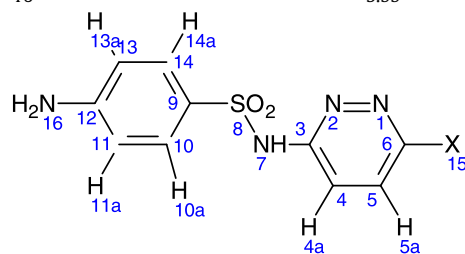
* Chemical shift of exchangeable protons in d$_6$-DMSO.

3.6. Sulfachloropyridazine reaction product

Fig. 9 shows the evolution of sulfachloropyridazine concentration in water at 65 °C in the presence of mordenite.

Surprisingly, after a few days, the formation of a unique reaction product was revealed. The ^{1}H NMR spectrum of the reaction product in CH$_3$OD is similar to that of the parent compound, probably indicating structure resemblance, in that it retains the presence of one AA'XX' aromatic system (6.67 and 7.56 ppm) and one AB aromatic system (6.95 and 7.50 ppm) (Table 5). More signals belonging to exchangeable protons appear when the reaction product is dissolved in d$_6$-DMSO (Fig. 3S in additional information), namely, an NH$_2$ group at 5.99 ppm, a broad NH signal at 10.57 ppm and an additional exchangeable signal integrating for one proton at 12.36 ppm; the latter is diagnostic of a hydroxyl group, probably substituting for chlorine at position 15 of the pyridazine ring (see Table 5 for atom numbering of sulfachloropyridazine reaction product in CD$_3$OD and d$_6$-DMSO). Hydroxyl for chlorine substitution can be proved by comparing the gHMBC spectrum of the reaction product to the one of the parent antibiotic in CD$_3$OD (Fig. 4S and 5S in additional information): apparently, the former shows clear connectivity between the pyridazine proton at 7.50 ppm and a carbon at 162.8 ppm, while no such carbon signal is present in the latter spectrum. Moreover, only the chemical shifts of the pyridazine moiety are affected by substitution, whereas the chemical shifts of the other ring do not change (Table 5).

In addition, the typical isotopic mass pattern of chlorine atom was absent in the mass spectrum. In the light of the GC–MS and NMR results the reaction product was undoubtedly identified as 4-amino-*N*-(6-hydroxyl-3-pyridazinyl)benzene sulfonamide (see structure in Table 1). The same structure has been proposed in a previous work on the basis of MS spectra of degradation products obtained by electrochemical destruction of sulfachloropyridazine [42].

The antibiotic concentration trend at 65 °C (Fig. 9) can be described as a two step process. In the first step, the concentration decreases rapidly up to 12 h (ca. 30% of the initial value), mainly because of the drug adsorption into HS-MOR. In the second step,

the concentration decreases very slowly and after 50 days becomes ca. 19% of the initial value. In the same time interval, the formation of the reaction product continuously increases in the contact solution.

At different time intervals, mordenite samples were isolated from the aqueous solution and extracted with methanol. The presence of sulfachloropyridazine in the extractant was revealed by HPLC analysis, whereas no reaction product was found. IR analysis performed on mordenite samples after methanol extraction showed the spectra of bare zeolite (spectra not shown).

In aqueous solution at pH 4.0 (pH value of the mordenite-antibiotic solution), the antibiotic was stable for several weeks, thus ruling out any hydrolytic or microbial degradation mechanism responsible for the formation of the new product.

The reaction product can be formed via nucleophilic aromatic substitution (S$_N$Ar) mechanism where the leaving group chloride is formerly displaced by hydroxyl anion (HO$^-$) nucleophile. The attempt to synthesize the reaction product in water at pH 10 (pH value at which the hydroxyl anion concentration should be high enough for the chlorine displacement) was not successful owing to the negative nature of sulfachloropyridazine (pKa = 5.5, Table 1) at that pH. In Scheme 2, the resonance structures of deprotonated antibiotic are shown.

Clearly, structures I and II are unfavourable to the displacement of chlorine atom. Therefore, despite the high concentration of hydroxyl anions at pH 10, the sulfachloropyridazine negative form at that pH does not allow the S$_N$Ar mechanism.

According to S$_N$Ar mechanism, the chlorine substitution can take place in case a net or partial positive charge is stabilized on the nitrogen of the heterocyclic ring at one atom distance from C–Cl (N1 according to the numbering reported in Table 5), and this is the case when sulfachloropyridazine is H-bonded to silanol groups as represented in Scheme 3, in agreement with the observation that silanols are perturbed by sulfachloropyridazine adsorption (Fig. 8, curve c). Because Rietveld analysis indicates that the heterocyclic ring enters inside the side pocket, we can safely propose that the silanols are located inside the side pocket: this is in
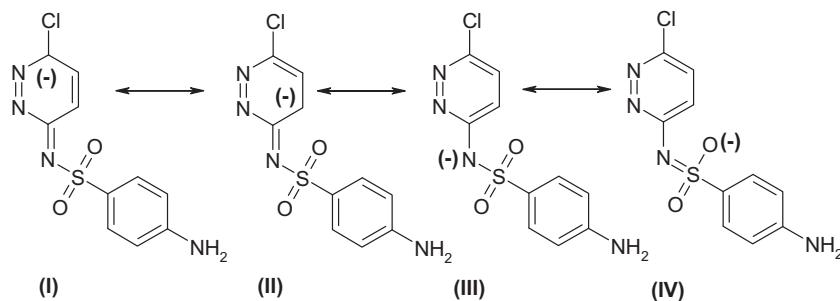
Scheme 2. Resonance forms of deprotonated sulfachloropyridazine (pKa = 5.5). Forms I and II are unfavourable to nucleophilic aromatic substitution (S_NAr) to pyridazine ring.
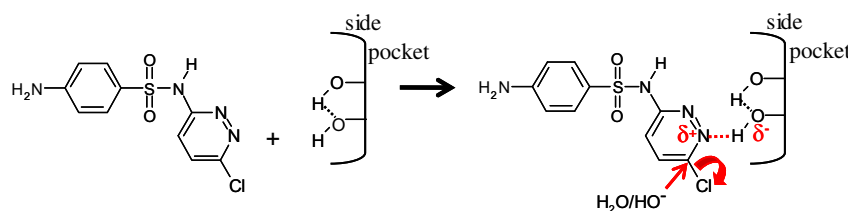
Scheme 3. Nucleophilic aromatic substitution (S_NAr) mechanism proposed for the formation of sulfachloropyridazine reaction product. The H-bond between mordenite vicinal silanol groups and pyridazine ring nitrogen atoms leads to a partial positive charge on the pyridazine ring that favours the displacement of the chloride leaving group.

agreement with the observation that the dealumination leads to an enlargement of the side pockets [1].

In summary: (i) sulfachloropyridazine irreversibly adsorbs by aqueous solution into mordenite via H-bonding with silanol groups located into the side pockets; (ii) a prolonged contact with mordenite in aqueous media at 65 °C leads to a single reaction product by S_NAr mechanism where chlorine is displaced by an –OH group; (iii) the product does not remained adsorbed into mordenite and easily migrate to the aqueous media owing to its increased hydrophilicity.

In a previous study [7], no sulfachloropyridazine transformation product was observed when the antibiotic was irreversibly adsorbed into high silica zeolite Y by water at 65 °C. In fact, no H-bond between pyridazine ring and zeolite Y silanol fraction was revealed by infrared analysis [8]. Very likely, not only the presence of silanols in mordenite, but also the specific constrain offered by its channel side pocket, favours the intimate interaction of the sulfa drug pyridazine ring with the silanols contained in that specific spatial region.

Consequently, because of the shape and size of the sulfachloropyridazine molecule, an anisotropic change in the geometry of mordenite channel systems has to be expected. As mentioned in the introduction section, only small molecule such as methane or acetonitrile can enter into mordenite side pocket [2,43]. Likely, the dealumination should lead to side pockets enlargement to contain the antibiotic heterocycle, and this can occur assuming a merging of vicinal pockets with part of the main channel [1]. The accessibility of bulky molecules as iso-propylamine or *tert*-butyl pyridine to mordenite side pockets has been observed after dealumination of mordenite [44,45].

4. Conclusions

A commercial high silica mordenite characterised by 200 SiO_2/Al_2O_3 was selected to test the adsorption of sulfachloropyridazine antibiotic by water at room temperature. The adsorption kinetics was favourable being complete within 4 h with an antibiotic maximal adsorption capacity of about 15% zeolite dry weight. The adsorption observed was fully irreversible in water.

In water at 65 °C the parent antibiotic transformed with slow kinetics but 100% selectivity to a new sulfonamide structure where the chlorine atom is displaced by an oxydryl group. The reaction product preserves the structure of the parent drug and might have some value as antibiotic itself.

In the present study, the mechanism proposed for the formation of the reaction product is a nucleophilic aromatic substitution (S_NAr) taking place on the pyridazine ring of the sulfa drug H-bonded to mordenite silanols through the ring nitrogen atoms. The stabilization of partial positive charges on the heterocyclic ring after antibiotic adsorption into mordenite accounts for the chlorine displacement.

The occurrence of H-bonds between pyridazine ring nitrogen atoms and mordenite silanols were found by FTIR and elucidated by the position of adsorbed antibiotic obtained by Rietveld analysis of XRPD data. The embedding of sulfachloropyridazine induced a combined effect of widening/contraction of all channel systems, which was highlighted by the variations of O–O distance of both 12 and 8MRs to favour the adsorption of the drug.

Sulfachloropyridazine was localised with the pyridazinyl ring oriented towards the mordenite side pocket with distances between ring nitrogen atoms and mordenite silanols typical of medium strength H-bond. The strength of these H-bonds was also evaluated by infrared analysis depending on the position of silanol stretching bands after antibiotic adsorption in comparison with the isolated silanol stretching mode. The IR spectrum of the adsorbed drug suggests the occurrence of a significant perturbation of the molecular and electronic structure of the heterocyclic ring as a consequence of H-bonding between the heterocyclic ring and silanols located into mordenite side pocket.

is acknowledged for TGA. The constructive reviews of referees were highly appreciated.

Appendix A. Supplementary data

Supplementary data associated with this article can be found, in the online version, at http://dx.doi.org/10.1016/j.micromeso.2012.11.031.

References

[1] S. Ban, A.N.C. van Laak, J. Landers, A.V. Neimark, P.E. de Jongh, K.P. de Jong, T.J.H. Vlugt, J. Phys. Chem. C 114 (2010) 2056.
[2] V.R. Choudhary, S. Mayadevi, A.P. Singh, J. Chem. Soc. Faraday Trans. 91 (1995) 2935.
[3] J. Nagano, T. Eguchi, T. Asanuma, H. Masui, H. Nakayama, N. Nakamura, E.G. Derouane, Microporous Mesoporous Mater. 33 (1999) 249.
[4] P. Bodart, J.B. Nagy, G. Debras, Z. Gabelica, P.A. Jacobs, J. Phys. Chem. 90 (1986) 5183.
[5] N. Viswanadham, M. Kumar, Microporous Mesoporous Mater. 92 (2006) 31.
[6] A. Martucci, L. Pasti, N. Marchetti, A. Cavazzini, F. Dondi, A. Alberti, Microporous Mesoporous Mater. 148 (2012) 174.
[7] I. Braschi, S. Blasioli, L. Gigli, C.E. Gessa, A. Alberti, A. Martucci, J. Hazard. Mater. 17 (2010) 218.
[8] I. Braschi, G. Gatti, G. Paul, C.E. Gessa, M. Cossi, L. Marchese, Langmuir 26 (2010) 9524.
[9] A. Martucci, L. Pasti, M. Nassi, A. Alberti, R. Arletti, R. Bagatin, R. Vignola, R. Sticca, Microporous Mesoporous Mater. 151 (2012) 358.
[10] R. Arletti, A. Martucci, A. Alberti, L. Pasti, M. Nassi, R. Bagatin, J. Solid State Chem. 194 (2012) 135.
[11] L. Ji, W. Chen, S. Zheng, Z. Xu, D. Zhu, Langmuir 25 (2009) 11608.
[12] S. Fukahori, T. Fujiwara, R. Ito, N. Funamizu, Desalination 275 (2011) 237.
[13] W. Yang, F. Zheng, X. Xue, Y. Lu, J. Colloid Interface Sci. 362 (2011) 503.
[14] M. Kahle, C. Stamm, Chemosphere 68 (2007) 1224.
[15] M. Burkhardt, C. Stamm, C. Waul, H. Singer, S. Müller, J. Environ. Qual. 34 (2005) 1363.
[16] S. Thiele-Bruhn, J. Plant Nutr. Soil Sci. 166 (2003) 145.
[17] S. Thiele-Bruhn, T. Seibicke, H.R. Schulten, P. Leinweber, J. Environ. Qual. 33 (2004) 1331.
[18] F.C. Cabello, Environ. Microbiol. 8 (2006) 1137.
[19] J. Acar, B. Rostel, Rev. Sci. Tech. 20 (2011) 797.
[20] F.R. Ungemach, Acta Vet. Scand. Suppl. 93 (2000) 89.
[21] M.E. Lindsey, M. Meyer, E.M. Thurman, Anal. Chem. 73 (2001) 4640.
[22] A.B.A. Boxall, P.A. Blackwell, R. Cavallo, P. Kay, J. Tolls, Toxicol. Lett. 131 (2002) 19.
[23] S. Lowell, J.E. Shields, M.A. Thomas, M. Thommes, Characterization of Porous Solids and Powders: Surface Area, Pore Size and Density, third ed., Kluwer Academic Publishers, 2004.
[24] A. Boultif, D. Louër, J. Appl. Crystallogr. 24 (1991) 987.
[25] A.C. Larson, R.B. Von Dreele, General Structure Analysis System (GSAS), Los Alamos National Laboratory Report LAUR, 2000, pp. 86–748.
[26] B.H. Toby, J. Appl. Crystallogr. 34 (2001) 210.
[27] A. Alberti, P. Davoli, G. Vezzalini, Z. Kristallogr. 175 (1986) 249.
[28] P. Thompson, D.E. Cox, J.B. Hastings, J. Appl. Crystallogr. 20 (1987) 217.
[29] Y.-S. Tan, Z.-F. Chen, H. Liang, Y. Zhang, Acta Crystallogr. E61 (2005) 1842.
[30] National Aquaculture Association, Judicious Antimicrobial Use of US Aquaculture: Principles and Practices, 2003, pp. 1–5.
[31] A.K. Sarmah, M.T. Meyer, A.B. Boxall, Chemosphere 65 (2006) 725.
[32] P. Simoncic, T. Armbruster, Am. Mineral. 89 (2004) 421.
[33] J.L. Schlenker, J.J. Pluth, J.V. Smith, Mater. Res. Bull. 13 (1978) 169.
[34] J.L. Schlenker, J.J. Pluth, J.V. Smith, Mater. Res. Bull. 14 (1979) 751.
[35] P. Simoncic, T. Armbruster, Microporous Mesoporous Mater. 71 (2004) 185.
[36] P. Simoncic, T. Armbruster, Microporous Mesoporous Mater. 81 (1–3) (2005) 87.
[37] C.H. Baerlocher, L.B. McCusker, D.H. Olson, Atlas of Zeolite Framework Types sixth revised ed., Elsevier, Amsterdam, 2007.
[38] D.E. Cox, R.J. Papoular, Mater. Sci. Forum 228 (1996) 233.
[39] A. Zecchina, S. Bordiga, G. Spoto, L. Marchese, G. Petrid, G. Leofanti, M. Padovan, J. Phys. Chem. 96 (1992) 4991.
[40] I. Braschi, G. Gatti, C. Bisio, G. Berlier, V. Sacchetto, M. Cossi, L. Marchese, J. Phys. Chem. C 116 (2012) 6943.
[41] A. Novak, Hydrogen bonding in solids. Correlation of spectroscopic and crystallographic data, in: J.D. Dunitz, P. Hemmerich, K.R.H. Holm, J.A. Ibers, C.K. Jorgensen, J.B. Neilands, D. Reinen, R.J.R. Williams (Eds.), Structure and Bonding, vol. 18, Springer-Verlag, Berlin, Heidelberg, New York, 1974, pp. 177–216.
[42] A. Dirany, I. Sirés, N. Oturan, A. Özcan, M.A. Oturan, Environ. Sci. Technol. 46 (2012) 4074.
[43] V.D. Dominguez-Soria, P. Calamacini, J. Phys. Chem. C 115 (2011) 6508.
[44] M. Tromp, J.A. van Bokhoven, M.T. Garriga Oostenbrink, J.H. Bitter, K.P. de Jong, D.C. Koningsberger, J. Catal. 190 (2000) 209.
[45] N.S. Nesterenko, F. Thibault-Starzyk, V. Montouillout, V.V. Yuschenko, C. Fernandez, J.-P. Gilson, F. Fajula, I.I. Ivanova, Microporous Mesoporous Mater. 71 (2004) 157.